This article has been accepted for publication in a future issue of this journal, but has not been fully edited. Content may change prior to final publication. Citation information: DOI 10.1109/TIA.2019.2920227, IEEE Transactions on Industry Applications

ZERO CURRENT SWITCHING RESONANT CONVERTER BASED PARALLEL BALANCING OF SERIALLY CONNECTED BATTERIES STRING

I. Zeltser[*], M. Evzelman[§], *Member, IEEE,* A. Kuperman[※], *Senior Member, IEEE,* M. M. Peretz[§], *Member, IEEE*

[*] Power Electronics Department, Rafael Advanced Defense Systems, P.O. Box 2250, Haifa 3102102, Israel, ilyaz@rafael.co.il

[§] PEMIC, Dept. of Electrical and Computer Eng., Ben-Gurion University of the Negev, P.O. Box 653, Beer-Sheva 84105, Israel, evzelman@bgu.ac.il, morp@bgu.ac.il,

[※]Applied Energy Laboratory, Dept. of Electrical and Computer Eng., Ben-Gurion University of the Negev, P.O. Box 653, Beer-Sheva 84105, Israel, alonk@bgu.ac.il

***Abstract* -- This paper introduces a new zero current switching (ZCS) topology for parallel balancing of serially connected batteries string. The main advantage of the balancing concept in this study is that energy is transferred only when the cells are unbalanced. As a result, the power losses are significantly reduced since no current circulates through the system when balanced. This has been enabled by a modification of an isolated series-resonant converter operating in discontinuous conduction mode (DCM). A single transformer for two cells is used, as opposed to conventional isolated topologies that require a transformer per cell. The realization is simple and sensorless. Experimental results have been obtained by a prototype of two modules balancing 4 series connected batteries.**

***Index Terms*--Batteries, balancing, soft switching, resonant converter.**

I. INTRODUCTION

Serially connected batteries strings have been used for many high voltage DC applications. Among them, electric vehicles (EV) [2], hybrid electric vehicles (HEV) [3], plug-in hybrid electric vehicle (PHEV) [4] and other battery powered applications [5], [6]. Due to manufacturing and environmental variances, degradation with aging, internal impedance difference and thermal conditions, the charges transferred to or consumed from each battery are not equal. As a result, the lifetime and efficiency of the batteries string are reduced. Moreover, the overcharge of the batteries in the string can cause explosion or fire in the case of sensitive batteries cells [7]. Therefore, a charge equalizer (i.e., balancing circuit) is essential to reduce the imbalances and consequently to improve the overall performance of the system [8], [9].

Several balancing circuits have been investigated over the recent years [10]-[34]. These can be generally divided into two main categories: passive and active. Passive balancing features simple design and implementation and relatively low cost [10], but due to inherent energy loss, it is less attractive in terms of energy saving. The active balancing architectures include variety of topologies such as switched-capacitor converters [11]-[13], [38], isolated and non-isolated unidirectional and bidirectional DC-DC converters [14]-[25], and multi-winding transformer-based converters [26]-[28].

An important classification of the active balancing circuits is in the power flow architecture, i.e., series balancing and parallel balancing. In series balancing, e.g. as in [12]-[13] and [22]-[23], energy is transferred from one neighboring cell to another using a power converter that links between two adjacent cells, and acts as a local bypass to the energy flow, in case a cell is damaged or has lower energy. Parallel balancing is assisted by a small energy storage component, typically a capacitor, and often referred as energy buffer, which is used as a link to transfer energy from a charged cell to the cell that needs to be charged without the need to process the energy through the whole batteries string [25], [31]. Therefore, an apparent advantage of the parallel balancing approach is the fewer amount of conversions to balance the string and as a result faster balancing with higher efficiency especially in large arrays. However, the penalty is often the requirement of high component count and complex control algorithms which increase the complexity (and cost) of the solution. In addition, increasing the balancing speed is traded for quiescent power losses, i.e. losses that exist when no balancing action is required. Similar parallel balancing concepts were reported for PV solar panels equalization under different names, [39]-[41], such as “returned path” in [39] and “DC power optimizers” in [40]. However the principal of operation, and consequently the advantages and the down sides of the parallel balancing converter whether it is implemented using a switched capacitor, switched inductor, or transformer based converter are similar to each other.

Improved balancing schemes that are based on parallel balancing techniques, exhibited higher equalization speed when compared to series balancing techniques [31]. One particular challenge of the parallel balancing concept is the complexity in implementing large arrays. This has been addressed by a modularization concept presented in [32]-[35]. There, n-batteries string is divided into M modules, each of them is balancing K cells so that $n=M\cdot K$. It would be a further value if the balancing concept can be realized by converter configurations of lower quiescent power consumption and reduced component count. This has been pursued in this study.

The objective of this study is therefore to introduce a new converter topology for active parallel balancing of serially

This article has been accepted for publication in a future issue of this journal, but has not been fully edited. Content may change prior to final publication. Citation information: DOI 10.1109/TIA.2019.2920227, IEEE Transactions on Industry Applications

connected battery string, as detailed in Fig. 1. The concept is realized by a modification of an isolated series-resonant converter such that one transformer is used to balance two cells, reducing the component count and complexity of the system. The converter operates in DCM and therefore ZCS is assured. Balancing occurs only when necessary, i.e. energy does not circulate through the system when the batteries are balanced. As a result, the quiescent power loss is minimal, which contributes to the current balancing architecture efficiency. The balancing circuit is sensorless and the balancing control is simple. Moreover, the converter can be easily scaled up and modularized.

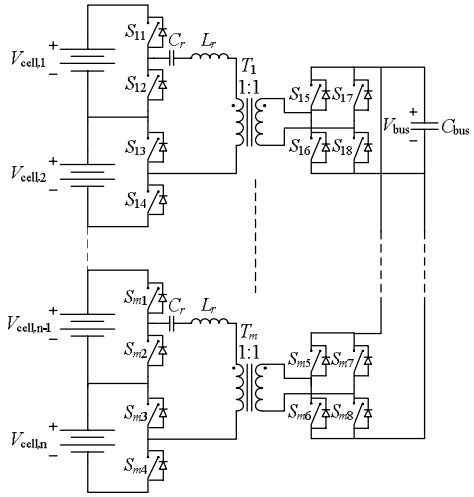

Fig. 1. Battery balancing system for *n* serially connected batteries.

The rest of the paper is organized as follows: Section II describes the topology, its principle of operation and the major features of it, Section III delineates the system's implementation and provides design guidelines. Experimental results and conclusion are then provided in Sections IV and V, respectively.

II. Principle of Operation

The system in Fig. 1 can be divided into $m = n/2$ double-cell modules, where each module is constructed of a top cell (odd-numbered cells) and a bottom cell (even-numbered cells). Each of the *m* double-cells is balanced using a module, constructed of a half-bridge loaded by a resonant tank in series with the primary side of the transformer. The secondary side connects to the bus capacitor via a full-bridge transistor assembly. The bus capacitor is common for all of the *m* double-cell modules and acts as a "link" that is used to transfer energy between the cells. Utilizing the isolation, each of the *n* battery cells can be equalized independently of the action in other cells, that is, no synchronization between the modules is required, and therefore the complexity of the system is significantly reduced. Additionally, due to the transformer's isolation, the voltage stress on the switches is no more than the cell's voltage and is independent on the number of cells in the string. The switching frequency f_s is set to be lower than half the resonant frequency f_r ($f_s<f_r$) to allow operation with ZCS.

The balancing time is shared equally between the odd and even numbered cells, i.e. the odd numbered cells are enabled to balance for a number of switching cycles and then the even numbered cells are enabled to balance for the same number of switching cycles, as shown in Fig. 2.

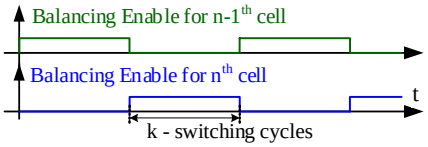

Fig. 2. Time shared cell balancing enable signals.

The balancing action resembles a conventional resonant converter in DCM. The operation of the switches is described in Fig. 3 for the upper cell, assisted by the switch sequences and current and voltage waveforms of Fig. 4. In the first step (time interval of half-switching period), switches S_{m1}, S_{m3}, S_{m5} and S_{m8} are turned on at $t=t_0$, and remain on for $t_0<t<t_1$ (Fig. 3(a), Fig. 3(e)), where $t_1<t_0+1/2f_r$, allowing bi-directional current flow. The current direction depends on the voltage difference between the battery cell voltage $V_{cell,n-1}$ and the bus voltage reflected to the primary (V_{bus} for the unity transformer ratio). Cell voltage that is higher than twice the bus capacitor voltage ($V_{cell,n-1}> 2V_{bus}$) results in a positive current i_r (Fig. 3(a); k=1 in Fig. 4), whereas $V_{cell,n-1}<2V_{bus}$, results in a negative current (Fig. 3(e); k=-1 in Fig. 4). In case that the cell voltage equals twice the bus capacitor voltage ($V_{cell,n-1}=2V_{bus}$), no balancing is needed, the current is zero and no energy is transferred in either direction.

In the second step (the second time interval of half-switching period), S_{m1}, S_{m5} and S_{m8} are turned off at t_1. For positive current ($V_{cell,n-1}> 2V_{bus}$), the body diodes of S_{m2}, S_{m5} and S_{m8} are conducting until the current becomes zero at $t_1=t_0+1/2f_r$ (Fig. 3(b)). It should be noted that turning S_{m1}, S_{m5} and S_{m8} off at a low, nonzero current (prior to t_1) further allows ZVS at turn off. Assuming that the voltage difference between half the cell voltage and the bus voltage, reflected to the primary, is small enough, the current remains zero until half of the switching period $t_2=t_0+1/2f_s$. At t_2 (See Fig. 3c)), S_{m2}, S_{m6} and S_{m7} are turned on and remain on for $t_2<t<t_3$, where $t_3<t_2+1/2f_r$. This discharges the resonant capacitor (Fig. 4). At t_3 (See Fig. 3(d), S_{m2}, S_{m6} and S_{m7} are tuned off and, if some residual current exists, it flows via the body diodes of S_{m1}, S_{m6} and S_{m7} until it becomes zero. The current remains zero until the next switching cycle at $t_4=t_0+1/f_s$.

When $V_{cell,n-1}< 2V_{bus}$, the resonant current during the time interval $t_0<t<t_1$ is negative and the operation is mirrored with respect to the cell and the bus side (See Fig. 3(e) - Fig. 3(h); and the case of k=-1 in Fig. 4). The body diodes of S_{m1}, S_{m6} and S_{m7} are conducting for $t_1<t< t_0+1/2f_r$, as shown in Fig. 3(f), and the diodes of S_{m2}, S_{m5} and S_{m8} during $t_3<t<t_3+1/2f_r$ (Fig. 3(h)). It should be noted that the switching sequence is similar regardless the difference between the cell and the bus voltages, for both positive and negative current. As a result, a sensorless operation can be utilized. In addition, the

This article has been accepted for publication in a future issue of this journal, but has not been fully edited. Content may change prior to final publication. Citation information: DOI 10.1109/TIA.2019.2920227, IEEE Transactions on Industry Applications

switching timing can be loosely set, because ZCS is naturally obtained by the body diodes as long as the switches have been turned off prior to the zero crossing point [36].

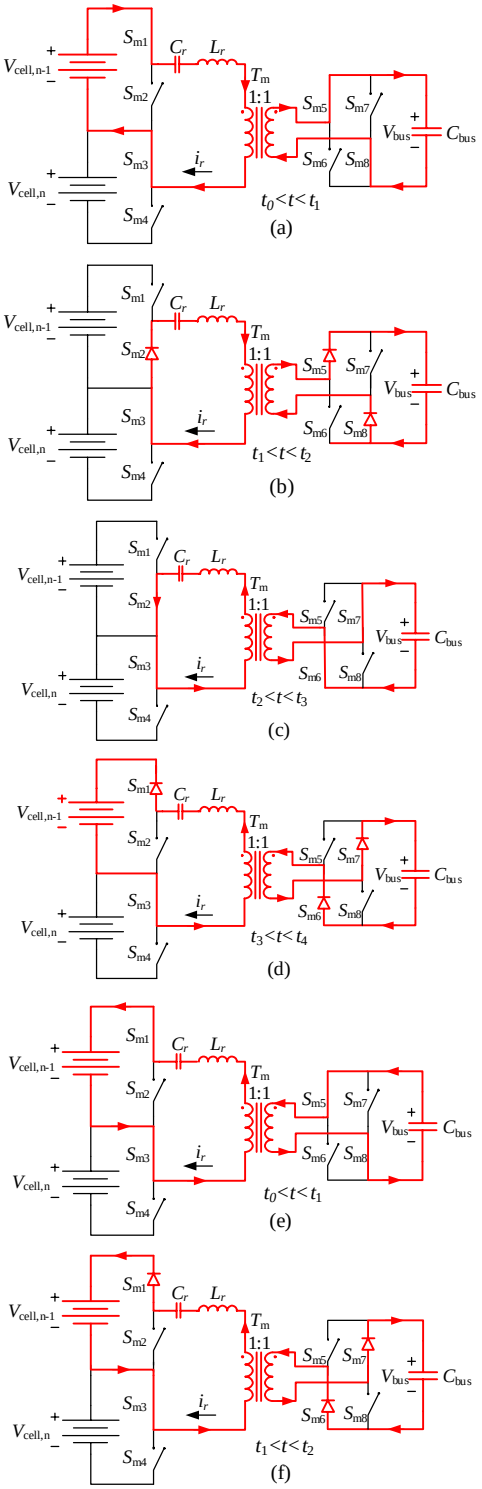

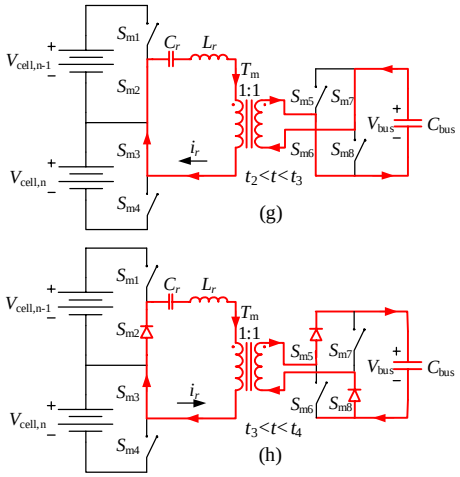

Fig. 3. Modes of operation: (a), (b), (c) and (d) when $V_{cell,n-1} > 2V_{bus}$, (e), (f), (g) and (h) when $V_{cell,n-1} < 2V_{bus}$.

It should be stressed that all the switches in the proposed balancing circuit are operated under soft switching conditions at both turn-on and turn-off. Moreover, virtually no current is circulating in the circuit when the cells are balanced. This is unlike many balancers, described in the prior art, where the current is going back and forth even when the cells voltages are equal. Putting this in other words, during the equalization phase, the losses in the proposed balancer are similar to those found in isolated resonant converter, operated below the half of the resonant frequency (DCM). When the cells are balanced, the only losses present are hysteresis losses of the isolation transformer, as no current is circulating in the system.

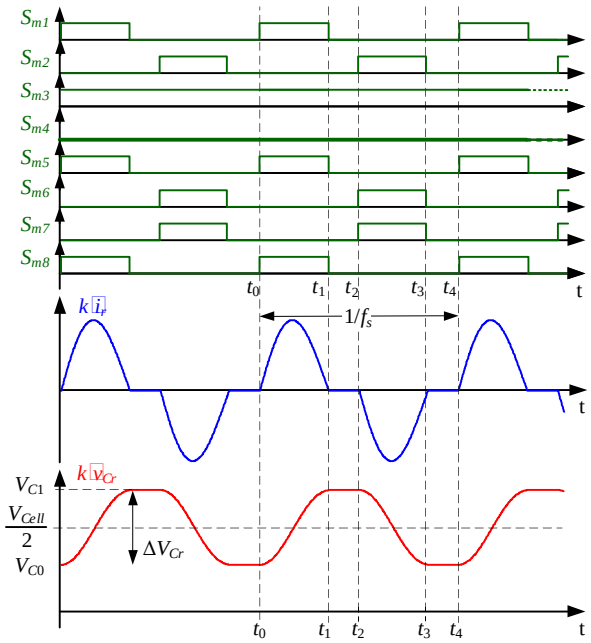

Fig. 4. Switching sequences and typical waveforms of the resonant inductor current and resonant capacitor voltage during balancing. k=1 when $V_{cell,n-1} > 2V_{bus}$ and k=-1, when $V_{cell,n-1} < 2V_{bus}$.

This article has been accepted for publication in a future issue of this journal, but has not been fully edited. Content may change prior to final publication. Citation information: DOI 10.1109/TIA.2019.2920227, IEEE Transactions on Industry Applications

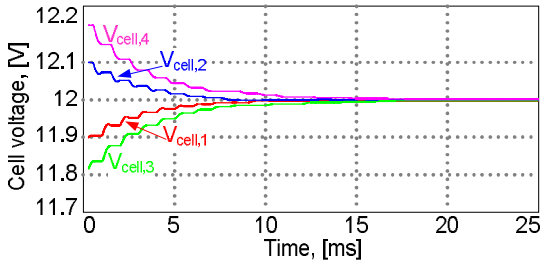

Fig. 5. Simulated convergence of cells with different initial voltage.

Simulated typical convergence during balancing operation of the system is presented in Fig. 5, where four battery cells (emulated by large capacitances) have been charged to different voltages. As can be observed, the cells voltages converge to the average of the initial voltages, validating the balancing operation of the system. The bus voltage converges to average of half the voltage levels of the cells in the pack, given by

$$V_{\text{bus}} = \frac{1}{2N}\sum_{k=1}^{N} V_{\text{cell},k}. \tag{1}$$

To derive the expressions for the system's key waveforms and parameters, it is assumed in the following analysis, that the cell voltage (V_{cell}) and the bus voltage V_{bus} are constant and that the average voltage across the resonant capacitor has reached a steady-state value of half the cell voltage, i.e. $V_{Cr}=0.5V_{\text{cell}}$. The cell is considered to be fully balanced when its voltage is equal to the twice the bus voltage, that is $0.5V_{cell}=V_{bus}$. Consequently, during the balancing operation, the normalized cell-to-bus voltage difference, which is defined here as $\Delta V=0.5V_{cell}-V_{bus}$, gradually decreases. It is further assumed that the capacitance of the bus capacitor is significantly lower than the cells' capacity. As a result, the bus voltage rapidly converges to the half of the average cells' voltages as in (1), which translates to a relatively small normalized cell-to-bus voltage difference during steady-state. The resonant current i_r can be expressed as

$$i_r(t)=\begin{cases}\dfrac{2\left(0.5V_{\text{cell}}-V_{\text{bus}}\right)}{\left(1-e^{-\frac{\pi}{2Q}}\right)Z_r}e^{-\frac{2\pi f_r}{2Q}t}\sin(2\pi f_r t), & t_0 \le t \le t_0+1/2f_r\\ \dfrac{2\left(V_{\text{bus}}-0.5V_{\text{cell}}\right)}{\left(1-e^{-\frac{\pi}{2Q}}\right)Z_r}e^{-\frac{2\pi f_r}{2Q}t}\sin(2\pi f_r t), & t_2 \le t \le t_2+1/2f_r\\ 0, & \text{elsewhere}\end{cases} \tag{2}$$

where, the resonant tank's characteristic impedance Z_r, resonant frequency f_r and the quality factor Q are

$$Z_r=\sqrt{\frac{L_r}{C_r}};\ f_r=\frac{1}{2\pi\sqrt{L_rC_r}};\ Q=\frac{1}{R}\sqrt{\frac{L_r}{C_r}} \tag{3}$$

and L_r and C_r are the resonant network components and R is the total parasitic or stray series resistance of the resonant loop.

From (2), the peak amplitude of the resonant current and the average current through the cell can be expressed as:

$$I_{\text{peak}}=\frac{2\left(0.5V_{\text{cell}}-V_{\text{bus}}\right)}{Z_r}\frac{e^{-\frac{\pi}{4Q}}}{1-e^{-\frac{\pi}{2Q}}}, \tag{4}$$

$$I_{\text{cell}}=\frac{\delta}{\pi}\frac{0.5V_{\text{cell}}-V_{\text{bus}}}{Z_r}\frac{1+e^{-\frac{\pi}{2Q}}}{1-e^{-\frac{\pi}{2Q}}}, \tag{5}$$

where $\delta=f_s/f_r$. The voltage swing of the resonant capacitor ΔV_{Cr} during one switching cycle $T_s=1/f_s$ can be expressed as:

$$\Delta V_{C_r}=2\left(0.5V_{\text{cell}}-V_{\text{bus}}\right)\frac{1+e^{-\frac{\pi}{2Q}}}{1-e^{-\frac{\pi}{2Q}}} \tag{6}$$

where, V_{C0} and V_{C1} are the initial and final voltages (Fig. 3), respectively, given by:

$$V_{C_0}=0.5(V_{\text{cell}}-\Delta V_{C_r}),\quad V_{C_1}=0.5(V_{\text{cell}}+\Delta V_{C_r}). \tag{7}$$

Assuming some given normalized cell-to-bus voltage difference ΔV, and considering that its change over the switching cycle is negligibly small, the power processing efficiency, defined over the switching period, can be expressed as

$$\eta=1-\frac{P_{\text{loss}}}{P_{\text{cell}}}\approx 1-\frac{P_{\text{cond}}}{P_{\text{cell}}}=1-\frac{8Q^2}{1+4Q^2}\frac{\Delta V}{V_{\text{cell}}} \tag{8}$$

where P_{cond} is the conduction losses and P_{cell} is the power generated by the cell.

As mentioned earlier and expressed by (1), the bus voltage converges to half of the cell's average voltage. This process can be assumed instantaneous when compared to the rate that cells' voltages vary. As can be seen in (8), the power processing efficiency linearly depends on ΔV, which reflects on the voltage difference between the cells. This implies that when balance is achieved the converter exhibits ideal power processing efficiency, a consequence of the fact that no current circulates through the system when balanced. It should be further noted that setting the resonant parameters reasonably high, ($Q > 1.6$), (8) can be approximated to:

$$\eta=1-2\Delta V\cdot V_{cell}^{-1}. \tag{9}$$

This highlights that the efficiency depends primarily on the cells' status, and is virtually independent on the system parameters, which is a clear advantage in any system and in particular for a system that comprises multiple converters or converters' string.

III. Implementation, Design Considerations and Topology Expansion

Implementation of each of the m modules in Fig. 1 is straightforward and is shown in Fig. 6. The battery cell side is built around a conventional resonant half-bridge converter topology whereas the bus capacitor side is constructed by a standard full-bridge rectifier. As a result, the design of the MOSFET's gate drivers is standard and comprises low-side and bootstrapped pairs. The design of the resonant inductance and transformer follows a classical integrated magnetic

This article has been accepted for publication in a future issue of this journal, but has not been fully edited. Content may change prior to final publication. Citation information: DOI 10.1109/TIA.2019.2920227, IEEE Transactions on Industry Applications

element design, where L_r can be the leakage inductance L_{lkg} of the transformer which has been estimated as described in [37].

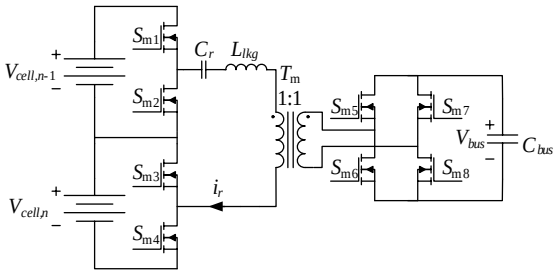

Fig. 6. Implementation of each of the *m* balancing circuits.

A. Design Considerations

The analysis derived earlier establishes the main attributes of the converter. Utilizing the above derivations, calculations of the key components of the converter can be established by the following procedure.

1. Choose target average current per cell I_{cell} for maximum setting of ΔV; the switching frequency f_s and the quality factor Q (Q should be larger than 1.6).
2. Calculate the expression

$$F(Q) = (1 + e^{-\frac{\pi}{2Q}})(1 - e^{-\frac{\pi}{2Q}})^{-1}. \tag{10}$$

3. From (5), (10), and considering δ < 1/2, L_r and C_r are selected according to

$$L_r < \frac{F(Q)\Delta V}{(2\pi)^2 I_{\text{cell}} f_s} \tag{11}$$

and

$$\left(\frac{\pi I_{\text{cell}}}{F(Q)\Delta V}\right)^2 L_r < C_r < \left(\frac{1}{2\pi f_s}\right)^2 \frac{1}{L_r}, \tag{12}$$

respectively.
4. Verify that the resonant tank's series resistance R satisfies

$$R < \frac{Z_r}{Q}. \tag{13}$$

If (13) does not hold, iterate (11) and (12).
5. The transformer's area of product $A_p^{'}$ (without the leakage inductance consideration) should be selected according to

$$A_p^{'} > \frac{V_{bus} \cdot I_{rms}}{\Delta B \cdot J \cdot K \cdot f_s} \tag{14}$$

where ΔB is the magnetic flux density at saturation, J is the current density and K is the winding fill factor.
6. One convenient way to achieve the desired leakage inductance L_{lkg} of the transformer is to place the windings as illustrated in Fig. 7 (for an E-type magnetic core). As described in [37], the leakage inductance in this case can be estimated by

$$L_{lkg} = \frac{\mu_0 n^2 ATL}{a}\left(\frac{b_1 + b_2}{3} + c\right)[H], \tag{15}$$

where μ_0 is the permeability constant, n is the number of turns in the primary winding, ATL is the average length of turn, a is the winding height (see Fig. 7), b_1 and b_2 are the thicknesses of the primary and secondary winding, respectively, and c is the distance between the primary and the secondary windings. All lengths are assigned in mm. In this study, the transformer has a 1:1 turns ratio and therefore b_1=b_2=b.

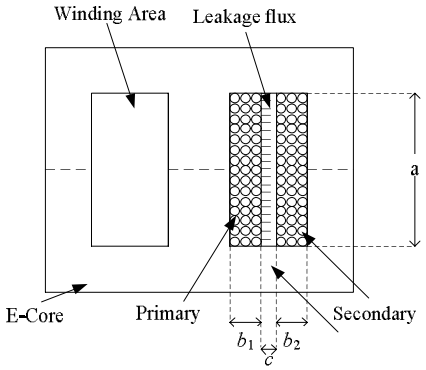

Fig. 7. Conventional transformer winding configuration for an E-core [37].

7. If c in (15) is non-zero, adjust the area product by

$$A_p = A_p'\left(1 + \frac{c}{2b}\right). \tag{16}$$

B. Practical implementation

The voltage stress of the transistors is the cell voltage for the cell side transistors and the bus capacitor voltage for the bus side. The lower voltage stress allows transistors with lower $R_{\text{DS(on)}}$ per silicon area. Current stresses depend on the desired
convergence speed. The isolation between the bus capacitor and the battery cells, provided by the transformer, enables the topology to be extended, as demonstrated in Fig. 8, for four battery cells. This modularization, as mentioned in [32], provides another stage of balancing which can expedite the balancing speed for the same power dissipation.

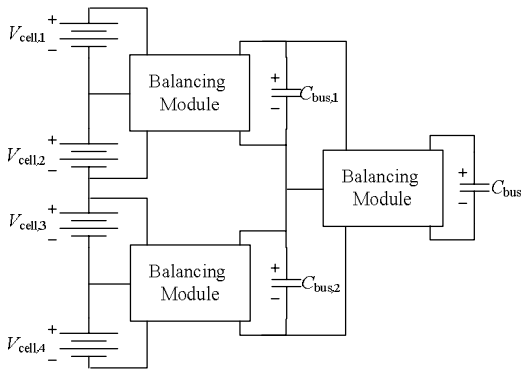

Fig. 8. Modularization of the balancing system for four battery cells.

Another option to implement the balancing architecture is by a multi-winding transformer for all or part of the modules as shown in Fig. 9 (instead of a transformer for each module). In this configuration, the overall component count of the system

This article has been accepted for publication in a future issue of this journal, but has not been fully edited. Content may change prior to final publication. Citation information: DOI 10.1109/TIA.2019.2920227, IEEE Transactions on Industry Applications

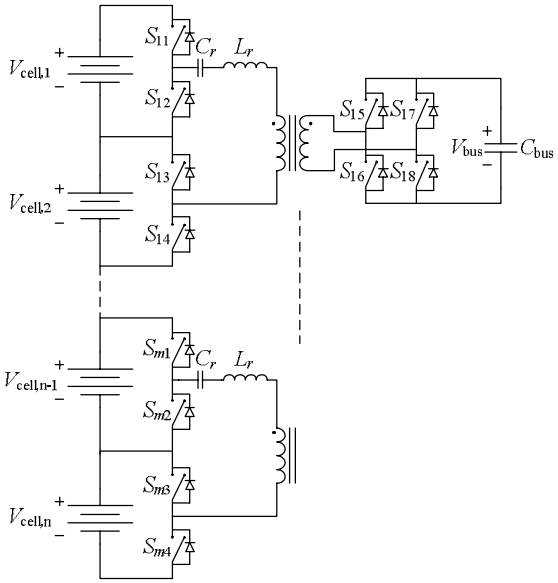

Fig. 9. Battery management system for n serially connected batteries, where multi-winding transformer is used for all modules.

is further reduced, where there one full bridge converter connects to the bus capacitor and one magnetic core (assuming the leakage inductance for each winding plays the role of the resonant inductor). The same principle of operation, expressions and parameters as described in Section II are applicable to the multi-winding configuration alternative. It should be noted however, that a design of such transformer may be complex in case that very large array is considered. To alleviate the challenges in construction of large arrays, multi-winding transformers can be designed for portions in the array, combining few modules together and utilizing modularization as described earlier by Fig. 8.

IV. Experimental Verification

The verification work of this study includes two levels of experimentation. One set of experiments has been conducted on a single module, to demonstrate the balancing action and verify the analytical predictions as well as the simulation results. This set uses two modules of the balancing system as described in Fig. 6. Each module consists of two battery cells (emulated by large capacitors). The modules are connected in series. The second set of experiments aimed at a larger scale, i.e. over several charging-discharging cycles, used to evaluate and quantify the benefits of the new balancing architecture. In these experiments, the battery string has been monitored for several cycles of 'routine' operation with and without the balancing system. To monitor the results over a wide time frame (approximately 40 hours per experiment), capture and log the data for variable charging and discharging patterns, an automated testing setup has been developed.

Experimental prototypes of two modules (Fig. 10) have been built and tested. Table I summarizes the component types and values used in the experimental prototype.

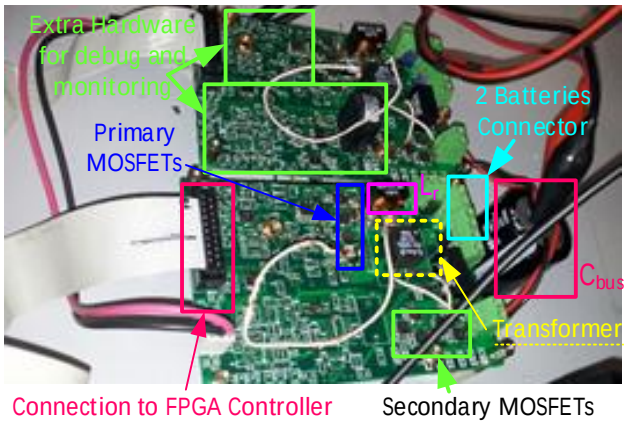

Fig. 10. Hardware prototype modules of the balancing system

The measured waveforms of the resonant tank during steady-state of the balancing operation are presented in Fig. 11. Based on the principle of operation described earlier, the balancing time is shared equally between the odd (*cell*,1 and *cell*,3) and the even (*cell*,2 and *cell*,4) numbered cells. The duration of each cell-balancing has been set to 200μs (i.e., the balancing time for the odd and even numbered cells), and cells' voltages have been preset to: $V_{cell,1}$ = 12V, $V_{cell,2}$ = 12.15V, $V_{cell,3}$ = 11.3V, $V_{cell,4}$ = 12.4V, therefore the average voltage of the pack is 11.95V. The procedure is demonstrated in Fig. 12, where the resonant current and the resonant capacitor voltage of both modules are measured over 500μs to include the balancing operation for the odd and the even numbered cells.

TABLE I
Experimental Prototype Parameters

Component	*Value*	*Quantity*
Cells: Batteries\capacitors	12 V, 5Ah \ 45mF	2
Transformer T_m, leakage inductance L_{lkg}	3.6 μH	1
Resonant tank capacitor C_r	250 nF	1
Transformer magnetizing inductance L_m	0.8 mH	-
MOSFETs S_{m1}-S_{m8}	Si4178DY	8
Bus capacitor C_{bus}	15 mF	1 shared
Resonant frequency f_r	168 kHz	-
Switching frequency f_s	130 kHz	-

During the first 200μs (second to fifth division in Fig. 12) the even numbered cells are balanced and the odd numbered cells are balanced in the successive 200μs. It can be seen that throughout the balancing of the even-numbered cells, the balancing current for *cell*,2 is lower than the balancing current for *cell*,4, since the voltage difference between $V_{cell,4}$ to the average voltage is greater than the respective voltage difference of $V_{cell,2}$. In the successive 200μs, *cell*,1 and *cell*,3, it can be observed that the balancing current of *cell*,1 is zero, since $V_{cell,1}$ equals to the average voltage of the string. Fig. 13 shows the cells' (realized by large capacitors to allow rapid convergence) voltages and the tanks' resonant currents over a long period of time when cells are pre-charged to different voltages. It can be observed that, the voltages of the four cells are equalized one to another and the currents decay to zero, verifying the analysis and simulation.

This article has been accepted for publication in a future issue of this journal, but has not been fully edited. Content may change prior to final publication. Citation information: DOI 10.1109/TIA.2019.2920227, IEEE Transactions on Industry Applications

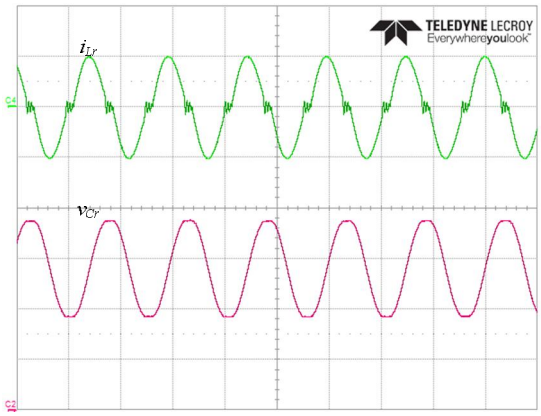

Fig. 11. Experimental results of resonant tank current (top) and resonant capacitor voltage (bottom) during balancing operation. Current 500mA/div, voltage 2V/div, time scale 5µs/div.

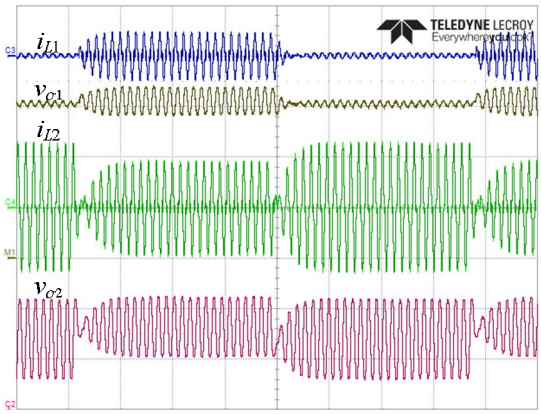

Fig. 12. Resonant tank current (top) and resonant capacitor voltage (bottom) during balancing of upper and lower cells with different voltages ($V_{cell,1}$ = 12V, $V_{cell,2}$ = 12.15V, $V_{cell,3}$ = 11.3V, $V_{cell,4}$ = 12.4V), each of them is balanced for 200 µs. Current 500mA/div, voltage 2V/div, time scale 50µs/div.

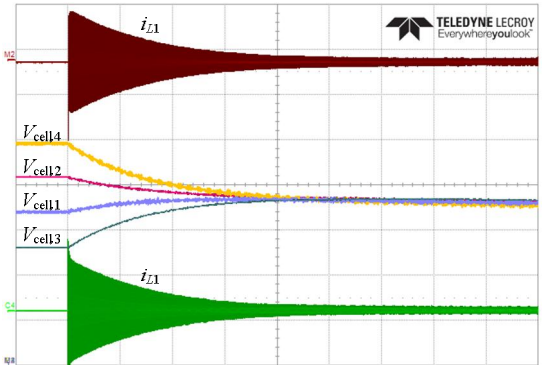

Fig. 13. Experimental results of voltage convergence of 4 cells with different initial voltages (F1 – $V_{cell,1}$, C2 – $V_{cell,2}$, M3 – $V_{cell,3}$, M4 – $V_{cell,4}$, C4 – i_{L1}, M2 – i_{L2}), and the tanks' resonant current. Time scale 200ms/div, Cells voltages 500mV/div, tanks' resonant current 500mA/div.

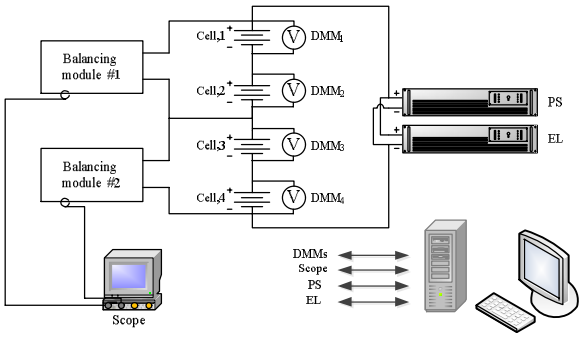

Fig. 14. A conceptual scheme of the automated setup used to generate the charge-discharge patterns, capture an log the data.

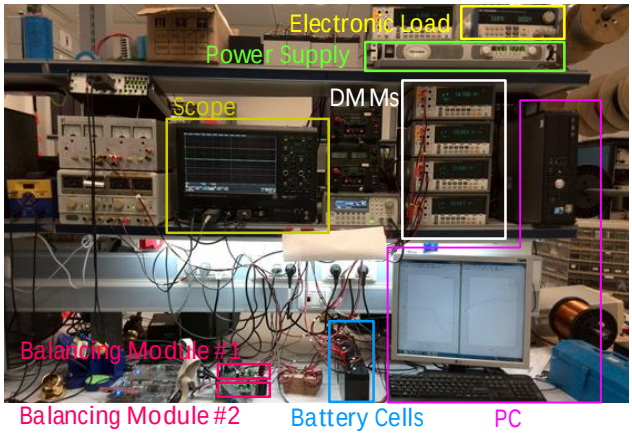

Fig. 15. Workstation of the automated testing setup for consecutive charge-discharge cycles.

The speed of cells convergence is regulated by the dead time between the charge/discharge instances of the resonant tank. The longer the dead time, the slower the speed of convergence. For wide time frame charging and discharging cycles experiments, four 12V, 5Ah (nominal), Lead-Acid batteries have been used as the series-connected battery string. An automated test bench as illustrated in Fig. 14, has been constructed to control the charging and discharging cycles and to acquire data from the battery string and from the balancing modules. The string has been tested with and without the balancing circuits. Fig. 15 shows a photograph of the automated testing setup.

Matlab code, running on the PC, controls the acquisition instruments, which comprises five DMMs measuring cells and bus voltages, programmable power supply for charging the entire string, an electronic load discharging it, and two current probes, connected to the scope measuring the balancing current of each balancing module. Lab equipment types that were used for this setup are detailed in TABLE II.

TABLE II
AUTOMATED SETUP INSTRUMENTS

Testing device	Model
DMM	Fluke 8845A
Power Supply	TDK Lambda Gen100-7.5
Electronic Load	BK Precision 8502
Scope	Lecroy HDO 4034

This article has been accepted for publication in a future issue of this journal, but has not been fully edited. Content may change prior to final publication. Citation information: DOI 10.1109/TIA.2019.2920227, IEEE Transactions on Industry Applications

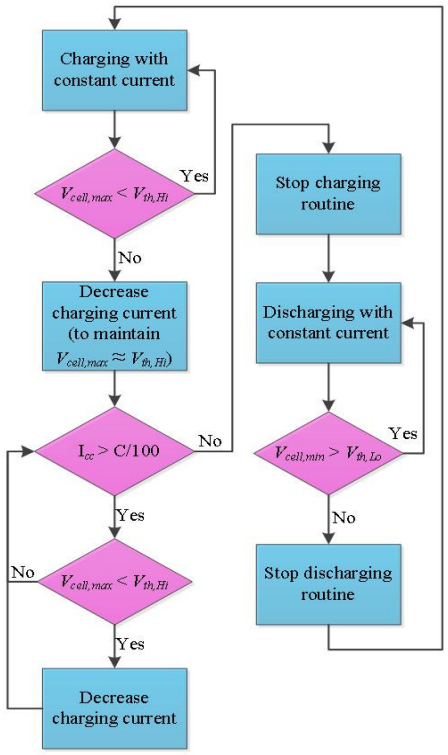

Fig. 16. Flow chart of MATLAB routine code.

A flow chart of the Matlab code routine that controls the charging and discharging cycles of the series-connected battery string with and without the balancing modules is shown in Fig. 16. *C* refers to the charging current that will charge a fully discharged cell to it's full capacity (5Ah in this case) in one hour. I_{CC} refers to a constant charging current provided to the cells. The cut-off voltages for charging and discharging are $V_{th,Hi}$ (14.8V) and $V_{th,Lo}$ (10.5V), respectively.

Prior to the following experiment, that utilizes the flow described in Fig. 16, each battery is charged to its maximum (CC/CV charging method). Then, the batteries are individually fully discharged. By doing so and bearing in mind that the initial SoC for all the cells is virtually identical, their actual capacity could be extracted. It is found to be approximately 3.1Ah. In the next step, the cells are charged with different amount of charge: *cell*,1 = 0.525Ah, *cell*,2 = 0.35Ah, *cell*,3 = 0.175Ah and *cell*,4 is not charged at all. This is intentionally done to set different SoC values for each cell. The constant current for charging and the discharging is set to 0.2C (1A).

The experiment includes 5 charge/discharge cycles. In the first cycle (cycle 0), the balancing circuit is turned off, during the rest of the cycles (cycle 1 to cycle 4) the balancing circuit is active. One-hour idle time is added between the cycles to allow cell relaxation processes to conclude so that cell's SoC could be reliably estimated from open-circuit cell voltage readings. The charging current and the cells' voltages are shown in Fig. 17 and Fig. 18 respectively. Once the balancing circuits are turned on, cycle 1, the voltages begin to converge to each other, and during the last cycle, cycle 4 the voltages are virtually equalized. Table III summarizes the amount of energy extracted from the battery string with and without the balancing circuits.

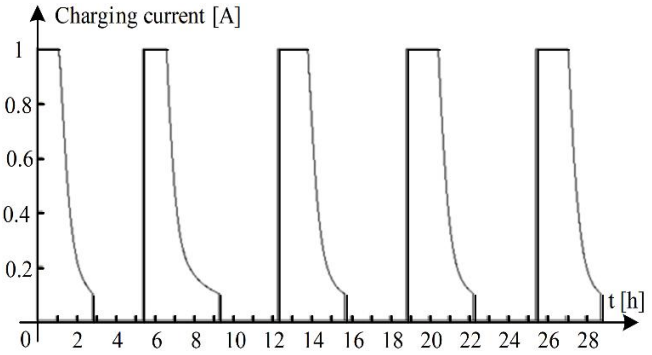

Fig. 17. Experimental results of the charging current for 4 Lead-Acid batteries string during charge-discharge cycles

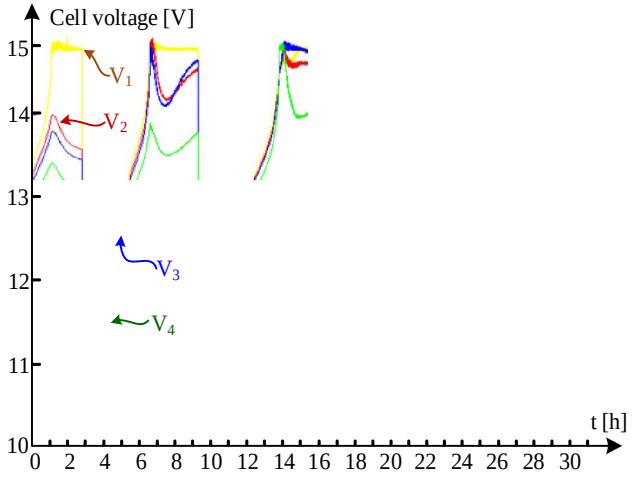

Fig. 18. Experimental results of the cell voltages of 4 Lead-Acid batteries string during charge-discharge cycles with and without balancing system.

TABLE III
ENERGY IMPROVEMENT PER CYCLE

Cycle	Discharge Time [h]	Extracted Energy [Wh]	Improvement over preceding cycle [%]	Overall improvement [%]
0	1.58	78.55	-	0
1	2.02	99.92	27.2	27.2
2	2.14	106.21	6.3	33.5
3	2.17	107.81	1.5	35
4	2.19	109.1	1.1	36.1

Cycle 0 (the balancing circuits are deactivated) is used as a reference. Immediately with activation of the balancing circuits, at cycle 1, the energy that was extracted from the string was increased by 27.2% as compared to the reference cycle. In the next cycle, cycle 2, 6.3% more energy was extracted than in cycle 1, and in cycle 3 and cycle 4 1.5% and 1.1% more energy was extracted than in the preceding cycle respectively. Overall, the activation of balancing circuits have improved battery string performance in terms of energy

extraction by 36.1% after the 4th cycle, comparing to the capability of the battery string without the balancing circuitry, i.e. the energy extracted during cycle 0.

V. Conclusion

In this work, a new soft switched isolated balancing topology and operation method have been introduced. The circuit is based on a modified series resonant converter operating in DCM. The new balancing circuit uses one transformer for balancing of two neighboring cells and as a result, less magnetic components are required compared to other isolated balancing topologies. Another significant advantage of the topology is the extremely low quiescent losses and as a result balancing system efficiency due to the native behavior of the converter where no current circulates through the system when the cells are balanced. Furthermore, the topology can be easily scaled-up and modularized for as many cells as required. A hardware prototype has been built and tested verifying the balancing operation, analysis and simulation. For an actual unbalanced batteries string, substantial improvement, in terms of discharged energy and discharge time, is observed after applying the balancing circuit.

References

[1] N. Dahan, O. Kirshenboim, I. Zeltser, and M. M. Peretz, "ZCS resonant converter based parallel balancing of serially connected batteries string," in Proc. IEEE Appl. Power Electron. Conf. Expo., pp. 802-809, Mar. 2016.

[2] A. Emadi, L. Young Joo, and K. Rajashekara, "Power electronics and motor drives in electric, hybrid electric, and plug-in hybrid electric vehicles," *IEEE Trans. Ind. Electron.*, vol. 55, no. 6, pp. 2237–2245, Jun. 2008.

[3] M. Ehsani, G. Yimin, J. M. Miller, "Hybrid electric vehicles: architecture and motor drives," *Proceedings of the IEEE*, vol. 95, no. 4, pp. 719-728, Apr. 2007.

[4] A. Y. Saber and G. K. Venayagamoorthy, "Plug-in vehicles and renewable energy sources for cost and emission reductions," *IEEE Trans. Ind. Electron.*, vol. 58, no. 4, pp. 1229–1238, Apr. 2011.

[5] H. Qian, J. Zhang, J. S. Lai, and W. Yu, "A high-efficiency grid-tie battery energy storage system," *IEEE Trans. Power Electron.*, vol. 26, no. 3, pp. 886–896, Mar. 2011.

[6] B. Gu, J. Dominic, B. Chen, and J. S. Lai, "A high-efficiency single-phase bidirectional AC-DC converter with minimized common mode voltages for battery energy storage systems," in *Proc. IEEE Energy Convers. Congr. Expo. 2013*, pp. 5145-5149, Sep. 2013.

[7] B. T. Kuhn, G. E. Pitel, and P. T. Krein, "Electrical properties and equalization of lithium-ion cells in automotive applications," in *Proc. IEEE Vehicle Power Propuls. Conf.*, pp. 55–59, Sep. 2005.

[8] P. T. Krein and R. S. Balog, "Life extension through charge equalization of lead–acid batteries," in *Proc. Int. Telecommun. Energy Conf. (INTELEC)*, pp. 516–523, 2002.

[9] M. Uno and K. Tanaka, "Influence of high-frequency charge–discharge cycling induced by cell voltage equalizers on the life performance of lithium-ion cells," *IEEE Trans. Veh. Technol.*, vol. 60, no. 4, pp. 1505–1515, May 2011.

[10] J. Cao, M. Schofield and A. Emadi, "Battery balancing methods: A comprehensive review," *IEEE Vehicle Power and Propulsion Conference, VPPC '08*. pp.1,6, Sep. 2008.

[11] A. C. Baughman and M. Ferdowsi, "Double-tiered switched-capacitor battery charge equalization technique," *IEEE Trans. Ind. Electron.*, vol. 55, no. 6, pp. 2277-2285, Jun. 2008.

[12] C. Pascual and P. T. Krein, "Switched capacitor system for automatic series battery equalization" in *Proc. IEEE Appl. Power Electron. Conf. Expo. 1997*, pp. 848-854, Feb. 1997.

[13] M. W. Cheng, Y. S. Lee, R. H. Chen, and W. T. Sie, "Cell voltage equalization using ZCS SC bidirectional converters," in *Proc. Int. Telecommun. Energy Conf.*, pp. 1–6, Oct. 2009.

[14] F. Mestrallet, L. Kerachev, J. C. Crebier and A. Collet, "Multiphase interleaved converter for lithium battery active balancing," *IEEE Trans. Power Electron.*, vol. 29, no. 6, pp. 2874-2881, Jun. 2014.

[15] L. Wang, L. Wang, C. Liao, and J. Liu, "Research on battery balance system applied on HEV," *VPPC '09*, pp. 1788-1791, Sep. 2009.

[16] Z. Nie and C. Mi, "Fast battery equalization with isolated bidirectional DC-DC converter for PHEV applications," *IEEE Vehicle Power and Propulsion Conference, VPPC '08*, pp. 78-81, Sep. 2009.

[17] Y. S. Lee and G. T. Cheng, "Quasi-resonant zero-current-switching bidirectional converter for battery equalization applications," *IEEE Trans. Power Electron.*, vol. 21, no. 5, pp. 1213-1224, Sep. 2006.

[18] M. Uno and K. Tanaka , "Single-switch cell voltage equalizer using multistacked buck-boost converters operating in discontinuous conduction mode for series-connected energy storage cells," *IEEE Trans. Vehicular Technology*, vol. 60, no. 8, pp. 3635-3645, Oct. 2011.

[19] M. Uno and K. Tanaka, "Single-switch multi-output charger using voltage multiplier for series-connected lithium-ion battery/supercapacitor equalization," *IEEE Trans. Ind. Electron.*, vol. 60, no. 8, pp. 3227–3239, Aug. 2013.

[20] G. Oriti, A. L. Julian and P. Norgaard, "Battery management system with cell equalizer for multi-cell battery packs" in *Proc. IEEE Energy Convers. Congr. Expo. 2014*, pp. 900-905, Sep. 2014.

[21] M. Uno and K. Tanaka, "Single-switch cell voltage equalizer using voltage multipliers for series-connected supercapacitors," in *Proc. IEEE Appl. Power Electron. Conf. Expo*, pp. 1266-1272, Feb. 2012.

[22] Y. Yuanmao, K. W. E. Cheng, and Y. P. B. Yeung, "Zero-current switching switched-capacitor zero-voltage-gap automatic equalization system for series battery string", *IEEE Trans. Power Electron.*, vol. 27, no. 7, pp. 3234-3242, Jul. 2012.

[23] C. H. Sung, K. Lee, and B. Kang, "Voltage equalizer for li-ion battery string using LC series resonance," *IECON 2013 - 39th Annual Conference of the IEEE*, pp.1404-1409, Nov. 2013.

[24] A. L. Julian, G. Oriti, M. E. Pfender, "SLR converter design for multi-cell battery charging," in *Proc. IEEE Energy Convers. Congr. Expo.*, pp. 743-748, Sep. 2013.

[25] D. Costinett, K. Hathaway, M. U. Rehman, M. Evzelman, R. Zane., Y. Levron, and D. Maksimovic, "Active balancing system for electric vehicles with incorporated low voltage bus," in *Proc. IEEE Appl. Power Electron. Conf. Expo. 2014*, pp. 3230-3236, Mar. 2014.

[26] S. Li, C. C. Mi and M. Zhang, "A high-efficiency active battery-balancing circuit using multiwinding transformer," *IEEE Trans. Ind. Applications*, vol. 49, no. 1, pp. 198-207, Jan. 2013.

[27] S. H. Park, K. B. Park, H. S. Kim, G. W. Moon, M. J. Youn, "Single-magnetic cell-to-cell charge equalization converter with reduced number of transformer windings," *IEEE Trans. Power Electron.*, vol. 27, no. 6, pp. 2900-2911, Jun. 2012.

[28] M. Y Kim, J. H. Kim, G. W. Moon, "Center-cell concentration structure of a cell-to-cell balancing circuit with a reduced number of switches," *IEEE Trans. Power Electron.*, vol. 29, no. 10, pp. 5285–5297, Oct. 2014.

[29] Y. S. Lee and M. W. Cheng, "Intelligent control battery equalization for series connected lithium-ion battery strings," *IEEE Trans. Ind. Electron.*, vol. 52, no. 5, pp. 1297-1307, Oct. 2005.

[30] M. U. Rehman, F. Zhane, M. Evzelman, R. Zane, and D. Maksimovic, "Control of a series-input, parallel-output cell balancing system for electric vehicle battery packs", *IEEE 16th Workshop on Control and Modeling for Power Electronics 2015*, Jul. 2015.

[31] B. Dong, Y. Li and Y. Han, "Parallel architecture for battery charge equalization," IEEE Trans. Power Electron., vol. 30, no. 9, pp. 4906-4913, Sep. 2015.

[32] H. S. Park, C. H. Kim; K. B. Park, G. W. Moon and J. H. Lee, "Design of a charge equalizer based on battery modularization," *IEEE Trans. Vehicular Technology*, vol. 58, no. 7, pp. 3216-3223, Sep. 2009.

[33] H. S. Park, C. E. Kim, C. H. Kim, G. W. Moon and J. H. Lee, "A modularized charge equalizer for an HEV lithium-ion battery string," *IEEE Trans. Ind. Electron.*, vol. 56, no. 5, pp. 1464-1476, May 2009.

[34] C. H. Kim, M. Y. Kim, and G. W. Moon, "A modularized charge equalizer using a battery monitoring IC for series-connected Li-ion battery

strings in electric vehicles," *IEEE Trans. Power Electron.*, vol. 28, no. 8, pp. 3779–3787, Aug. 2013.

[35] M. U. Rehman, M. Evzelman, K. Hathaway, R. Zane, G. L. Plett, K. Smith, E. Wood, and D. Maksimovic, "Modular approach for continuous cell-level balancing to improve performance of large battery packs," in *Proc. IEEE Energy Convers. Congr. Expo 2014*, pp. 4327-4334, Sep. 2014.

[36] E. Hamo, M. Evzelman, M. M. Peretz, "Modeling and analysis of resonant switched-capacitor converters with free-wheeling ZCS," *IEEE Trans. Power Electron*., vol. 30, no. 9, pp. 4952–4959, Sep. 2015.

[37] C. M. T. McLyman, "Winding capacitance and leakage inductance", Chap. 17, *Transformer and Inductor Design Handbook*, 3rd Ed. NY, Marcel Dekker, 2004.

[38] M. Uno and A. Kukita, "Charge equalizer using a Cockcroft-Walton vottage multiplier for series-connected supercapacitors," *INTELEC 2009 - 31st International Telecommunications Energy Conference*, Incheon, 2009, pp. 1-5.

[39] Y. Nimni and D. Shmilovitz, "A returned energy architecture for improved photovoltaic systems efficiency," *Proceedings of 2010 IEEE International Symposium on Circuits and Systems*, Paris, 2010, pp. 2191-2194.

[40] A. Elrayyah, M. Badawey and Y. Sozer, "Feeding partial power into line capacitors for low cost and efficient MPPT of photovoltaic strings," *2016 IEEE Applied Power Electronics Conference and Exposition (APEC)*, Long Beach, CA, 2016, pp. 392-397.

[41] Hurng-Liahng Jou, Kuen-Der Wu, Jinn-Chang Wu, Cheng-Huan Chung and Ding-Feng Huang, " Voltage Equalizing of Solar Modules for Shadowing Compensation," *Journal of Power Electronics*, vol. 17, no. 2, pp. 392-397, 2017.